

Why does sleep slow wave activity increase after extended wake?

Assessing the effects of increased cortical firing during wake and sleep

Alexander V. Rodriguez^{1,2}, Chadd M. Funk^{1,2,3}, Vladyslav V. Vyazovskiy⁴, Yuval Nir^{5,6},
Giulio Tononi¹ and Chiara Cirelli^{1*}

¹ Department of Psychiatry, University of Wisconsin-Madison, 6001 Research Park Blvd, Madison, WI 53719 USA

² Neuroscience Training Program, University of Wisconsin-Madison, 9531 WIMR II, 1111 Highland Ave, Madison, WI 53705 USA

³ Medical Scientist Training Program, University of Wisconsin-Madison, Health Sciences Learning Center, 750 Highland Ave, Madison, WI 53705, USA

⁴ Department of Physiology, Anatomy and Genetics, University of Oxford, Oxford, OX1 3PT, United Kingdom.

⁵ Sagol School of Neurosciences, Tel Aviv University, Tel Aviv, 69978, Israel

⁶ Department of Physiology and Pharmacology, Sackler School of Medicine, Tel Aviv University, Tel Aviv, 69978, Israel

Title: 21 words

Abstract: 233; Significance statement: 119; Introduction: 600; Discussion: 1459

4 Figures; 0 Tables; Pages: 24

Key words: fatigue, NREM sleep, cerebral cortex, optogenetics, sleep deprivation, mouse

Abbreviated Title: Determinants of slow wave homeostasis

Correspondence:

Chiara Cirelli, M.D., Ph.D.

Department of Psychiatry, University of Wisconsin - Madison

6001 Research Park Blvd

53719 Madison, Wisconsin, USA

ccirelli@wisc.edu

Conflicts of interest. G. Tononi is involved in a research study in humans supported by Philips Respironics. This study is not related to the work presented in the current manuscript. The other authors have indicated no financial conflicts of interest.

Acknowledgements. Supported by NIH grants 1R01MH091326 (GT), 1R01MH099231 (GT, CC) and 1P01NS083514 (GT, CC). We thank Dr. Ofer Yizhar (Weizmann Institute of Science, Rehovot, Israel) for valuable input regarding the use of SSFO.

Abstract

During NREM sleep cortical neurons alternate between ON periods of firing and OFF periods of silence. This bistability, which is largely synchronous across neurons, is reflected in the EEG as slow waves. Slow wave activity (SWA) increases with wake duration and declines homeostatically during sleep, but the underlying mechanisms remain unclear. One possibility is neuronal ‘fatigue’: high, sustained firing in wake would force neurons to recover with more frequent and longer OFF periods during sleep. Another possibility is net synaptic potentiation during wake: stronger coupling among neurons would lead to greater synchrony and therefore higher SWA. Here we obtained a comparable increase in sustained firing (six hours) in cortex by: i) keeping mice awake by exposure to novel objects to promote plasticity; ii) optogenetically activating a local population of cortical neurons at wake-like levels during sleep. Sleep following extended wake led to increased SWA, higher synchrony, and more time spent OFF, with a positive correlation between SWA, synchrony, and OFF periods. Moreover, time spent OFF was correlated with cortical firing during prior wake. After local optogenetic stimulation, SWA and cortical synchrony decreased locally, time spent OFF did not change, and local SWA was not correlated with either measure. Moreover, laser-induced cortical firing was not correlated with time spent OFF afterwards. Overall, these results suggest that high sustained firing per se may not be the primary determinant of SWA increases observed after extended wake.

Significance statement

A long-standing hypothesis is that neurons fire less during slow wave sleep to recover from the “fatigue” accrued during wake, when overall synaptic activity is higher than in sleep. This idea, however, has rarely been tested and other factors, namely increased cortical synchrony, could explain why sleep slow wave activity is higher after extended wake. We forced neurons in the mouse cortex to fire at high levels for six hours in two different conditions, during active wake with exploration, and during sleep. We find that neurons need more time OFF only after sustained firing in wake, suggesting that fatigue due to sustained firing alone is unlikely to account for the increase in slow wave activity that follows sleep deprivation.

Introduction

During NREM sleep, cortical and thalamic neurons oscillate between ON states of firing and OFF periods of silence (Steriade et al., 2001, Chauvette et al., 2011). This bistability occurs more or less synchronously in many neurons and is recorded in the electroencephalogram (EEG) as slow waves. During NREM sleep, amplitude and incidence of slow waves are quantified using slow wave activity (SWA), the EEG power in the 0.5-4.0 Hz range. SWA increases with wake duration, peaks in early sleep and declines in late sleep. SWA is considered an index of the homeostatic process “S”, reflecting the increase in sleep need/intensity with wake duration (in conjunction with the circadian factor “C”, which affects primarily sleep timing and duration) (Borbély, 1982, Borbely et al., 2016).

However, the mechanisms linking wake duration to SWA remain unclear. Early hypotheses included the possible accumulation of “an endogenous sleep compound which is eliminated or inactivated during sleep” (Borbely et al., 1981) or of “metabolic processes” that need to be reversed in sleep (Feinberg et al., 1978). A long-standing hypothesis is that during wake neurons may accrue ‘fatigue’ due to overall higher firing, which would be reversed in NREM sleep as a result of reduced firing during OFF periods (Rechtschaffen, 1998, Vyazovskiy and Harris, 2013). Neuronal fatigue is usually conceptualized as temporary exhaustion triggered by intense activity, due to momentary run-down of energy resources (e.g. glycogen (Dalsgaard and Secher, 2007)), depletion of synaptic vesicles/calcium (O'Donovan and Rinzel, 1997), or accumulation of adenosine (Brundege and Dunwiddie, 1998, Brambilla et al., 2005, Lovatt et al., 2012). Indeed, it was explicitly suggested that SWA may reflect the build-up of adenosine and the subsequent potentiation of potassium currents that hyperpolarize cortical neurons during the OFF state (Benington and Heller, 1995).

Another hypothesis is that wake would lead to an overall increase in synaptic strength associated with learning, and that sleep would then be required to renormalize synaptic weights, with beneficial effects both at the cellular level (energy, supplies) and at the systems level (memory) (Cirelli et al., 2004, Tononi and Cirelli, 2006, 2012, 2014). The increase in SWA after wake would be due primarily to the increase in neuronal synchrony brought about by stronger synaptic coupling, just as its decrease during sleep would be due to reduced synchrony following net synaptic depression. The net increase in synaptic strength during wake and its decrease during sleep is

supported by molecular, electrophysiological, as well as structural and ultrastructural evidence (Tononi and Cirelli, 2014, de Vivo et al., 2016). Moreover, computer simulations show that increased synaptic strength is sufficient to cause higher synchrony, higher SWA, as well as more numerous and prolonged OFF periods (Esser et al., 2007). Accordingly, the onset of ON and OFF periods is more synchronous after extended wake and less so after sleep (Vyazovskiy et al., 2009).

So far, many studies have demonstrated a global increase in SWA after extended wakefulness with object exploration, and local increases after specific learning tasks (Hanlon et al., 2011). However, the relative contribution of increased neuronal firing and synaptic plasticity to subsequent SWA cannot easily be disentangled. The occurrence of OFF periods during wake ('local sleep') after extended exploration of novel objects (Vyazovskiy et al., 2011) could also reflect either fatigue due to excessive firing and/or excessive synaptic potentiation. In this work, we set out to test directly whether a sustained increase in mean cortical firing rate during wake, obtained by having animals explore novel objects to promote plasticity, and a comparable increase obtained by optogenetic stimulation during sleep, lead to differential effects on neuronal synchrony, SWA, and OFF periods during subsequent NREM sleep.

Material and Methods

Surgery. Adult (~60-90 days old) male transgenic B6.Cg-Tg(Camk2a-Cre)T29-1Stl/J mice that express Cre recombinase in excitatory cortical neurons were used (JAX Stock number 005359, Jackson Laboratory). Animals were housed in single cages and kept on a 12h:12h light/dark cycle with lights on at 10am. All animal procedures and experimental protocols followed the National Institutes of Health Guide for the Care and Use of Laboratory Animals and were approved by the licensing committee. All animal facilities were reviewed and approved by the institutional animal care and use committee (IACUC) of the University of Wisconsin-Madison, and were inspected and accredited by association for assessment and accreditation of laboratory animal care (AAALAC).

Virus injection and electrode implantation were performed in 2 separate surgeries, as adeno-associated viruses take up to 3 weeks to become fully expressed and cortical electrodes have a limited viable recording time once implanted, due to immune responses or glial buildup (Grill, 2008). Thus, we waited 3 weeks after virus injection before performing the electrode implant surgery. Both surgeries were performed under isoflurane anesthesia (2% for induction, 1-2% for

maintenance) using proper sterile technique. After making a small craniotomy in the skull, the purified adeno-associated virus rAAV5-Ef1a-DIO hChR2 (C128S/D156A-EYFP) (4×10^{12} virus particles/ml) was stereotactically injected into the right frontal cortex (from bregma, +1.28 A/P; +1.0 M/L; -1.5 D/V) at 0.1 μ L/min for 20 min (total 2 μ L of virus), with a 10-min wait following the end of the injection to allow for liquid diffusion into the cortex. This stable step function opsin (SSFO) virus was obtained from the UNC vector core (University of North Carolina, Chapel Hill, NC) under an agreement with Dr. Karl Deisseroth at Stanford University. The small craniotomy was covered using the dental acrylic Fusio (Pentron Clinical) and the incision was closed using Vetbond (3M). For chronic polygraphic recordings, gold screws were inserted into the skull above left frontal (+1.4 AP, -1.5 M/L) and right parietal cortex (-2.5A/P, +1.7 M/L) to record EEG activity, and stainless steel wires were implanted into the nuchal muscles for electromyography (EMG). Moreover, a microwire electrode array with 16 electrodes (Tucker-Davis Technologies) cemented to an optic fiber ferrule (Doric Lenses) was inserted into the right frontal hemisphere (+1.0 A/P; +1.0 M/L; -1.4 D/V; D/V measured from cortex), along with a laminar probe (Neuronexus) or a second microwire array into the left parietal cortex. Arrays were targeted to the deep cortical layers (mainly layer 5), while laminar probes spanned all layers. After one week of recovery from the second surgery, animals were connected to a wire bundle to record electrical signals and an optic patch cable to prepare for laser stimulation. Using the RZ2 amplifier and PZ2 pre-amplifier (Tucker-Davis Technologies), EEG (256 Hz, bandpass filtered at 0.1-100 Hz) and EMG (256Hz, bandpass filtered at 10-50 Hz) signals were continuously collected for several weeks, together with local field potentials (LFPs, 256 Hz, bandpass filtered at 0.1-100 Hz) and multiunit activity (MUA, 24.4kHz, bandpass filtered at 300-5000 Hz). Thresholds for MUA were set manually below 0 mV, and waveforms for each threshold-crossing event were saved. Experiments started only after the sleep/wake cycle had normalized and mice were fully entrained to the light/dark cycle, sleeping mostly during the day and staying awake mainly at night. Percentage of sleep and wake (mean \pm std) during the light phase in baseline were consistent with published values (e.g. (Franken et al., 1999, Huber et al., 2000, Bellesi et al., 2015)): Wake: $39.8\% \pm 5.0\%$, NREM sleep: $50.5\% \pm 4.6\%$, REM sleep: $9.7\% \pm 1.6\%$.

Sleep Deprivation (SD). SD was performed for 6 hours starting at light onset using exposure to novel objects. Since the procedure can be stressful in naïve animals, mice were familiarized with the

method by placing a new object in the cage every day for several days prior to the SD experiment. During SD, mice were given a new object or bedding every time they were inactive and slow waves became evident on real-time EEG monitoring. Mice were never disturbed when they were spontaneously awake, feeding, or drinking. As some mice continue to stay awake for variable amounts of time after all objects are removed, analysis started always at hour 7, but the exact time was adjusted to begin at the onset of consolidated sleep, defined as the first 30-min window in which sleep accounted for at least 50% of the time, and whose first 3 minutes also included at least 50% of time spent asleep.

Laser Stimulation during NREM sleep (laser-S). To activate the stable step-function opsin (SSFO) rAAV5-Efla-DIO-hChR2 (C128S/D156A)-EYFP a 473 nm wavelength laser (OEM Laser Systems) was used. Laser stimulation was delivered remotely by an investigator who was outside the room housing the mice and was checking the polygraphic traces online. Short pulses of 2.3 ± 1.2 seconds (mean \pm std) in duration and ~ 1 mW in intensity (minimum 100μ W, maximum 15 mW, almost all pulses near 1 mW) were given approximately every 5 min, always during NREM sleep. Laser power and pulse timing were titrated to maintain wake-like, tonic firing in the stimulated electrodes. To match the SD experiment the overall duration of the laser-S experiment was 6 hours; the last pulse was given no later than 20 min before the end of the sixth hour to allow SSFO channels to close, thus reducing the risk of carryover effects.

Data Analysis. Frontal and parietal EEG and local field potentials (LFPs), as well as EMG waveforms were exported to the graphic interface SleepSign (Kissei Comtec), where 4-sec epochs were manually scored as wake, NREM sleep or REM sleep according to established criteria. In wake, muscle activity was high and the EEG was dominated by low amplitude, high frequency activity, while NREM sleep was characterized by low muscle tone and high amplitude, low frequency EEG/LFP activity, and REM sleep by low EMG activity with occasional twitches and strong theta (6-9 Hz) activity. Scoring could not be blind to experimental condition, given the obvious unique features of SD (continuous wake for 6 hours) and laser-S (high gamma power, see Results). All further analyses were performed using custom scripts in MATLAB (Mathworks). Fast Fourier transforms were calculated using Welch's approximation method on Hanning windows to gather power spectra data from 0 to 120 Hz for each 4-sec epoch. Multi-unit activity (MUA) was

down sampled into 2-ms bins (500 Hz) before all analyses (no spikes were lost due to down sampling). To calculate OFF period measures for MUA (number of OFF periods per minute of NREM sleep, average duration of OFF periods, and percent of time in NREM sleep spent OFF), each electrode was assigned an OFF period threshold, where all periods of silence equal to or longer than that threshold were counted as OFF periods. The OFF period threshold for an electrode was calculated by fitting the interspike intervals (ISIs) for an electrode to a gamma distribution using the MATLAB function ‘gamfit’. A number of ISIs equal to the number of ISIs used for fitting were drawn from this distribution, and the 99th percentile for ISI length from this set of ISIs was the OFF period threshold. A close variation of this process was used in previously published work (Vyazovskiy et al., 2011). However, the current analysis was performed at the single electrode level, whereas previously (Vyazovskiy et al., 2011) OFF measures were calculated on MUA collapsed across several electrodes (for validation of the current method, see Results). We also performed OFF period analysis on spike data collapsed across all electrodes of an array for each mouse. This collapsed spike train was then treated as firing from a single electrode, and the analysis was performed as above.

To calculate synchrony of ON periods between electrodes, contributing electrodes from each mouse were considered in groups. Each electrode from a mouse in turn was the ‘target’ electrode, while all other electrodes from the same array were ‘other’ electrodes (mice that contributed only one electrode were excluded from this analysis). ON periods were defined for each electrode as the entire time spent in NREM sleep that was not classified as an OFF period for that electrode (as defined above). The start of each ON period (that is, end of each OFF period) in the target electrode was the center of a time window of 48 ms. Other electrodes that also had ON periods starting within this 48 ms window were counted as ‘synchronous’. The proportion of other electrodes marked ‘synchronous’ provided a synchrony score for the beginning of each ON period in the target electrode. For example, if 4 of 4 other electrodes were synchronous, the score for that ON period was 1. If only 1 of 4 other electrodes were synchronous, the score was instead 0.25. The total synchrony score for an electrode was the average of the synchrony score across all of the ON period onsets for a given time period. This process was repeated for the ends of the ON periods.

Histology and colocalization studies. Mice were deeply anesthetized under 3% isoflurane and transcardially perfused with 0.9% saline followed by 4% paraformaldehyde (PFA) in phosphate

buffer. Brains were removed and placed in 4% PFA for at least 24 hours, then sliced into 50 μ m thick sections on a vibratome, covered in Vectashield (Vector Labs, H-1000), and imaged using a light microscope (Leica Microsystems) to verify virus expression and electrode placement in the cortex. To estimate the percentage of cells infected by the virus we injected 4 additional mice of the same strain, sex, and age as above with a nearly identical virus containing only EYFP (rAAV5-EF1a-DIO-EYFP). After allowing ~1 month for viral expression, mice were perfused and brains were sliced as above. A subset of slices was then selected for NeuN staining. Infection rate was estimated in the ‘main injection area’, which could be easily identified as the homogenous bright fluorescent area surrounding the injection. In all mice this region spanned more than 1 mm rostro-caudally, and corresponded to the area where the recording electrodes were located in implanted mice. To estimate the infection rate, we took 3 sections from each mouse within this area, 1 section that included the injection track, and 2 other sections located 0.5 mm rostral and 0.5 mm caudal to the central section. Sections were first left for 1 hour in 10% normal goat serum (NGS, MP Biomedicals 642921) in 0.05 M phosphate buffered saline (PBS), then incubated in rabbit anti-NeuN overnight at room temperature (Millipore ABN78, 1:200 in PBS). The next day, sections were washed 5 times for 5 min each in PBS and then left in 10% NGS for 25 min. Next, sections were incubated in anti-rabbit Alexa Fluor 568 for 1 hour at room temperature (Life Technologies A11011 1:1000 in PBS), then washed again, mounted onto glass slides and covered in Vectashield. One mouse was excluded due to faint viral expression. Within the remaining 3 mice, images from the main injection area of each section were taken using a confocal microscope (Olympus). Several (3 to 5) non-overlapping image stacks (5-10 μ m thick) were taken per section, depending on image quality and injection area, for a total of 39 stacks across the 3 mice. Images were analyzed with ImageJ using an algorithm that first collapsed stacks into a maximum projection, then automatically detected NeuN+ spots and marked them as regions of interest (ROIs). ROIs that contacted any of the 4 margins of the image were discarded, as mean EYFP fluorescence inside them could not be fully assessed. A fluorescence threshold was manually set after visual inspection and applied uniformly to all images. EYFP fluorescence was then measured across all ROIs. NeuN+ cells that contained an average EYFP fluorescence above threshold were counted as double-labeled (NeuN+ EYFP+) cells.

Results

261

262 We compared 2 experimental conditions associated with a similar sustained increase in cortical
263 neuronal activity, 6 hours of extended wake with exposure to novel objects, and 6 hours of
264 optogenetic stimulation of cortical pyramidal neurons during sleep. Twenty adult male Camk2a-Cre
265 mice were used in the study, all of which showed fairly widespread virus expression in the frontal
266 cortex, limited to the right hemisphere, and had microwire arrays well placed within the expression
267 area, as determined by histological examination (Figure 1A). The arrays in the right frontal cortex
268 each included 16 electrodes that are referred to as “ipsilateral” electrodes. These electrodes spanned
269 the cortical area injected with the virus that was subjected to optogenetic stimulation. Electrodes
270 placed in the left parietal cortex are referred to as “contralateral” electrodes (with neither viral
271 expression nor optogenetic stimulation; Figure 1B). The 16 ipsilateral electrodes were organized
272 into 2 parallel rows of 8 that spanned 1.4 mm in the anteroposterior direction and 0.5 mm
273 mediolaterally, and their tips were located at the same cortical depth, mainly in layer 5 (Figure 1B).
274 The extent of virus infection was estimated in 3 other Camk2a-Cre mice, not used for the 2 main
275 experiments, in which we counted how many cells in the main injected area expressed the neuronal
276 nuclear marker NeuN and contained rAAV5-EF1a-DIO-EYFP (see Methods for details). This virus
277 localizes throughout the cell, especially within the nucleus, and is almost identical to the one we
278 used for the laser experiment, whose expression is instead excluded from the nucleus (Yizhar et al.,
279 2011). In the 3 animals, $62.7 \pm 19.6\%$ of NeuN+ cells were also EYFP+ (39 images, mean \pm std;
280 Figure 1C), suggesting that, within the main injection area, most excitatory neurons were infected.

281 In each mouse, 2 experiments were performed: sleep deprivation (SD) and laser stimulation
282 during NREM sleep (laser-S), usually spaced \sim 4-5 days apart and run in counterbalanced order.
283 Both experiments lasted two days, with the first day being the baseline day in which mice were
284 allowed to sleep undisturbed (Figure 1D). On day two, during the first 6 hours of the light period,
285 mice were either kept awake by exposure to novel objects (SD) or allowed to sleep but received
286 laser stimulation during NREM sleep (laser-S). Sleep that followed SD or laser-S was analyzed
287 starting at hour 7 of the light period and compared to the same time period of the preceding baseline
288 day. Firing from all electrodes was manually inspected across both experimental days, and only
289 those electrodes that showed a stable signal across both days were selected for analysis. Most mice
290 (13 out of 20) contributed electrodes for both experimental conditions; in the remaining 7 mice, data
291 from only SD or laser-S could be used, due to decreased quality and stability of the recordings (see

below). Overall, 16 mice contributed data for SD, and 17 mice contributed for laser-S. Three measures were used to assess the effects of SD or laser-S: 1) the left frontal and right parietal EEG, to detect broad changes in brain activity outside the virus expression/stimulated area; 2) LFP recordings from ipsilateral and contralateral electrodes; 3) multi-unit activity (MUA) from the same electrodes.

Sleep deprivation increases cortical firing and is followed by increases in SWA and time spent OFF during sleep

SD by novel objects reduced the total time spent asleep to <1% of the 6 hours, with the few minutes of sleep spent in NREM sleep (not shown). To obtain an overall estimate of neuronal activity during SD we focused on the ipsilateral electrodes, the same ones targeted by laser stimulation (n=59, 16 mice), and for each of them we expressed the mean firing rate for hours 1-6 of the SD day as a percentage of the corresponding firing rate during hours 1-6 of the baseline day. In most electrodes, neuronal activity during SD increased relative to the same circadian time in baseline, when mice are mostly asleep. As a result, mean firing rate during SD increased by 72.13 ± 47.49 % (mean \pm std, 59 electrodes, 16 mice; Wilcoxon signed rank test, $p=2.65 \times 10^{-11}$; Figure 2A). Not surprisingly, a similar increase was present in contralateral channels (not shown).

As expected, mice showed a sleep rebound when they were allowed to sleep. During the first 2 hours after SD, time spent in NREM sleep increased at the expense of wake (% of time spent in each state, hours 7-8 of baseline day vs. hours 7-8 SD day, mean \pm std; wake: 37.5 ± 9.5 % vs. 17.6 ± 7.9 %, NREM: 52.1 ± 7.6 % vs. 71.8 ± 7.1 %, REM: 10.4 ± 2.8 % vs. 10.5 ± 2.7 %). SWA also increased at the beginning of the recovery period in both the left frontal EEG (Figure 2B) and the right parietal EEG (% increase in SD vs. baseline; 15 electrodes, 15 mice; 32.3 ± 23.3 %, mean \pm std; Wilcoxon signed rank test, $p=6.10 \times 10^{-5}$), and this increase was specific for the low EEG frequencies (Figure 2B). A similar specific increase in SWA was seen in the LFPs from all ipsilateral electrodes (Figure 2C). We then focused on measures of OFF periods (Figure 2D). First, we tested whether “OFF periods” as identified at the single-electrode level correspond to OFF periods as previously defined based on the positive peak of the LFP slow waves (negative peak of the scalp EEG slow waves), or on a pre-selected time of silence across all electrodes (Vyazovskiy et al., 2009). We found that this was the case. Specifically, we isolated single electrodes and examined the OFF period-triggered average of LFP traces and found that single-electrode OFF periods aligned

well with LFP positive peaks (Figure 2E). Next, to measure changes in neuronal activity during recovery sleep we calculated, for each ipsilateral electrode, the incidence of OFF periods (number/min of NREM sleep), their average duration, as well as the “percentage of time OFF” (total time spent in OFF periods, expressed as % of total time in NREM sleep) in hours 7-8 of the SD day, and compared these measures to the same circadian time in the baseline day (Figure 2D). Time spent in OFF periods increased in the first 2 hours following SD relative to the same circadian time in baseline, due to an increase in both number and duration of OFF periods (Figure 2F) and all changes had returned to baseline levels or lower by the first 2 hours of the dark period (Figure 2G). Moreover, time spent OFF in the first 2 hours after SD was correlated with mean firing rates during the 6 hours of extended wake (Figure 2H). Thus, after sustained high firing in wake for 6 hours, neurons spent more time OFF, a change that was reversible in a few hours. This change was detectable at the level of individual electrodes. We also calculated OFF period measures after collapsing all electrodes within each mouse and treating the collapsed MUA as a single MUA trace, similar to previous work (Vyazovskiy et al., 2009). Results were similar: number and duration of OFF periods, as well as percent of time spent OFF, significantly increased in hours 7-8 after SD relative to baseline (16 mice; mean \pm std, Wilcoxon signed rank test, N: $+10.1 \pm 17.9$ %; $p=0.03$; duration: $+7.3 \pm 9.2$ %; $p=0.008$; % OFF: $+18.8 \pm 24.5$ %; $p=0.009$). As previously reported in rats (Vyazovskiy et al., 2009), firing rate during the ON periods also increased in the first 2 hours after SD relative to baseline ($+7.2 \pm 11.9$ %; Wilcoxon signed rank test, $p=6.74 \times 10^{-5}$).

Laser stimulation during sleep increases local cortical firing without causing arousal, and is followed by a decrease in SWA and no changes in time spent OFF during sleep

The goal of the laser-S experiment was to force neurons in a small cortical area to fire during NREM sleep at levels comparable to those reached during SD, but without waking up the mice. Since high firing had to be maintained for several hours, a stable step function opsin (SSFO) was used, which introduces a steady cationic current into neurons and thus increases their overall excitability (Yizhar et al., 2011). An advantage of SSFOs is that affected neurons are more likely to still fire in their natural patterns, albeit at a higher rate, making the increased activity more physiologically relevant compared to repeated electrical stimulation or acute optogenetic stimulation using opsins with fast kinetics (Yizhar et al., 2011). Brief laser pulses (mostly ~ 2 sec at ~ 1 mW) were delivered only during NREM sleep, on average every 5 min, for a total of ~ 60 pulses

during hours 1-6 of the laser-S day. During this time, the percentage of wake, NREM sleep, and REM sleep did not differ from baseline (Figure 3A). The average duration of sleep and wake episodes, as well as number of brief awakenings (wake bouts of ≤ 16 sec), also did not change between hours 1-6 of the baseline and laser-S days (Figure 3A). SWA during NREM sleep showed a small but significant decrease in the ipsilateral (right) parietal EEG (percent change in laser-S vs. baseline = -7.4 ± 9.8 %; Wilcoxon signed rank test, $p=0.007$) and the contralateral (left) frontal EEG (Figure 3B), while gamma power was significantly increased in frontal EEG only (Figure 3B). In contrast to the small changes in global measures of sleep, laser stimulation clearly affected LFP spectral power and neuronal activity at the local level. As mentioned, we estimated that $\sim 63\%$ of neurons were infected with the virus in the main injected area, and because of the especially low power required for SSFO activation (Yizhar et al., 2011), and the fact that our laser light was focused on this area, we assume that most of them were activated. However, due to the complex nature of light diffusion within the cortex, we cannot estimate the total number of neurons activated by laser stimulation, nor can we be sure that all infected neurons were activated to the same extent. Indeed, the effects of the optogenetic stimulation varied across electrodes, either because of variable levels of virus expression and/or because of changes in light intensity at the different electrode sites. Thus, some electrodes were strong responders, showing a sustained increase in firing across the 6 hours, while others showed weak or no responses, or even a decrease in firing during laser stimulation (Figure 3C). When all ipsilateral electrodes were considered together ($n=66$, 15 mice) across the entire 6 hours, including both sleep and wake, there was an overall significant increase in mean firing rate of 53.6 ± 57.8 % relative to baseline (percent change hours 1-6 laser-S vs. hours 1-6 baseline, mean \pm std; Wilcoxon signed rank test, $p=8.82 \times 10^{-10}$). This increase, however, was significantly smaller than the increase seen during SD. Since matching the 2 experimental conditions (SD and laser-S) by overall increase in firing rate was key to the goal of the study, we then selected, among all ipsilateral electrodes ($n=66$), only those whose laser-induced increase in firing rate was within the mean \pm std observed during SD (72.1 ± 47.5 %). This selection resulted in 32 “SD-matched” electrodes, with an overall increase in mean firing rate of 66.1 ± 28.3 % (Figure 3D). During baseline, SD-matched electrodes did not show any obvious difference relative to the remaining ipsilateral electrodes: for instance, during hours 1-6 of the baseline day their mean firing rates and SWA power in NREM sleep varied within the same range as the other electrodes (not shown). During laser stimulation, firing in these SD-matched responders was wake-like with little

evidence of bistability, and indeed during the 6 hours of laser stimulation, the incidence of OFF periods during NREM sleep decreased by $\sim 90\%$ and the few remaining OFF periods were shorter, resulting in an almost complete lack of time OFF (Figure 3E). SD-matched electrodes also showed a noticeable shift in LFP power throughout the entire duration of the experiment, including a $\sim 30\%$ decrease in SWA and a $\sim 100\%$ increase in gamma power (Figure 3F). There was no correlation between changes in SWA and gamma power during the 6 hours of laser stimulation, and both changes were also visible in raw spectrograms in which LFP power was not normalized by the total power during baseline. During the 6 hours of laser stimulation contralateral channels showed no significant changes in firing rate ($3.0 \pm 15.8\%$, mean \pm std; Wilcoxon signed rank test, $p=0.36$), OFF measures (% OFF: $9.2 \pm 26.1\%$, $p=0.30$), or LFP SWA power ($1.1 \pm 6.4\%$, $p=0.50$) relative to baseline.

During the first two hours after laser-S (hours 7-8), SWA was slightly decreased in both left frontal EEG (Figure 3G) and right parietal EEG (not shown) as compared to baseline. The LFPs of the SD-matched channels no longer had elevated gamma power, but still showed a significant decline in SWA relative to baseline, albeit smaller than during stimulation (Figure 3H). As before, we found that OFF periods were well correlated with positive LFP peaks (Figure 3I). However, in SD-matched electrodes, none of the OFF measures changed significantly in the first two hours after Laser-S (Figure 3J), or later (not shown). Moreover, time spent OFF in the first 2 hours after laser stimulation did not correlate with mean firing rates during the 6 hours of optogenetic stimulation (Figure 3K). OFF measures also did not change if all ipsilateral electrodes were considered (Figure 3L). Electrodes placed in the contralateral parietal cortex, which received neither light exposure nor virus injection, showed no change in firing rate during laser-S ($3.0 \pm 15.8\%$, mean \pm std; Wilcoxon signed rank test, $p=0.36$), and no changes in OFF periods following laser stimulation (not shown). These results were confirmed when calculating OFF period measures after collapsing across all electrodes for each mouse (SD-matched electrodes, 11 mice; mean \pm std, Wilcoxon signed rank test; Number: $12.6 \pm 45.4\%$, $p=0.76$; Duration: $1.3 \pm 4.6\%$, $p=0.70$; % time OFF: 16.0 ± 53.4 , $p=0.64$). In contrast to the recovery sleep after SD, after laser stimulation, mean firing rates during the ON periods in hours 7-8 showed no change relative to baseline in SD-matched electrodes ($-1.9 \pm 14.4\%$; $p=0.21$).

Cortical synchrony increases after sleep deprivation but not after laser stimulation

Next we looked at the effects of SD and laser-S on neuronal coupling by measuring the extent to which the onset and offset of ON periods in each electrode were locked to those in the other electrodes of the same array (Figure 4A; see Methods for details). Consistent with previous work in rats (Vyazovskiy et al., 2009), neurons were significantly more likely to start and end their ON periods synchronously in the first 2 hours of recovery sleep after SD (Figure 4B; ON Starts, 48 ms window; 55 electrodes, 12 mice; 23.9 ± 31.8 %, mean \pm std; Wilcoxon signed rank test, $p=1.72 \times 10^{-6}$) and these results were robust across a series of time windows used to define synchronicity, from 48 ms to 148 ms. Moreover, SWA and synchrony measures were correlated (Figure 4C). By contrast, no increase in synchrony measures was seen after laser stimulation. In fact, the onset of the ON periods was significantly less synchronous across SD-matched electrodes (30 electrodes, 9 mice; -2.5 ± 25.8 %, mean \pm std; Wilcoxon signed rank test, $p=0.03$), and both onsets and offsets showed less synchrony when calculated across all ipsilateral electrodes (Figure 4D; 63 electrodes, 14 mice; 0.6 ± 25.6 %, mean \pm std; Wilcoxon signed rank test, $p = 0.001$). Thus, both SWA and synchrony measures decreased after optogenetic stimulation, but they were not correlated (Figure 4E). No changes were present in the contralateral electrodes (Figure 4F). The results again were confirmed using different time windows (100 and 148 ms, not shown).

Discussion

Changes in SWA and cortical synchrony after sleep deprivation

We measured sleep SWA, OFF measures and cortical synchrony i) after extended wake with exposure to novel objects and ii) after optogenetic cortical stimulation during NREM sleep. Both experimental conditions induced a comparable, sustained (6 hours) increase in mean cortical firing ($\sim 70\%$ relative to baseline). As expected, the increase in firing rate was widespread in both left and right cortex during sleep deprivation, and restricted to the targeted area during laser stimulation. The results show that sustained high firing induced by exposure to novel objects during wake was followed, during subsequent sleep, by an increase in SWA, cortical neuronal synchrony, and number and duration of OFF periods. Moreover, the increase in SWA was correlated with both neuronal synchrony and time spent OFF. These findings are fully in line with the results observed in the rat cortex (Vyazovskiy et al., 2009), confirming in two rodent species that homeostatic changes in SWA due to sleep deprivation are linked to changes in both cortical synchrony and OFF periods measures. Based on previous studies, we hypothesize that increased synchrony in the transition into

ON and OFF periods is a reflection of increased neuronal coupling due to net synaptic potentiation occurring during prior wake (Vyazovskiy et al., 2009, Tononi and Cirelli, 2014).

Changes in SWA and cortical synchrony after optogenetic stimulation during sleep

After laser stimulation high firing was confined to the main injection area, where we estimate that ~63% of neurons were infected by the virus. Of note, in the same area, and only during laser stimulation, we also found an increase in gamma power (Figure 3), which has frequently been observed as a result of inhibitory firing (Whittington et al., 2011, Buzsaki and Wang, 2012). Thus, although our stimulation targeted excitatory cells, most likely it also led to increased compensatory firing of fast spiking inhibitory interneurons, recruited to maintain the balance between excitation and inhibition.

None of the effects observed after sleep deprivation was observed following sustained firing induced by optogenetic stimulation during sleep: SWA and cortical synchrony decreased, the number and duration of OFF periods did not change, and SWA was not correlated with cortical synchrony and time spent OFF. Thus, a wake-like, tonic increase in firing comparable to that observed during active exploration, but produced by optogenetic activation during sleep, fails to trigger homeostatic changes in subsequent SWA and associated neural signatures. In fact, SWA and neural synchrony not only failed to increase, but declined significantly. Just like wake leads to a net increase in synaptic strength, presumably because of a neuromodulatory milieu that favors learning through synaptic potentiation, NREM sleep leads to a net decrease in synaptic strength, presumably through a neuromodulatory milieu that favors synaptic depression (Harley, 1991, Seol et al., 2007). It has been hypothesized that, at least in mammalian cortex, this sleep-dependent down-selection of synaptic strength would be activity-dependent (Tononi and Cirelli, 2014). Thus, we speculate that increased firing induced by optogenetic stimulation during sleep may have promoted additional synaptic depression, thereby explaining the decline in SWA and neuronal synchrony. In pilot experiments, optogenetic stimulation for several hours during wake, in conjunction with active exploration, often resulted in seizures or cortical spreading depression and prevented the analysis of subsequent sleep.

Mechanisms underlying the decline in SWA after optogenetic stimulation during sleep

In general, the synchrony of neuronal firing is strongly correlated with the amplitude of EEG signals (Musall et al., 2014). Since the effects of extended wake are global, they are expected to be similar, hence correlated, at every scale: from the synchrony of firing of the few units near the recording tip, to the amplitude of the local LFP, reflecting the input (mainly postsynaptic potentials) from thousands of neurons surrounding the recording electrode (Buzsaki et al., 2012), to the overall EEG. Indeed, extended wake increased both SWA and synchrony measures in a correlated manner, and the increase in SWA was also observed in the contralateral hemisphere, with no statistical differences between left and right cortex (Figure 2B,C). By contrast, optogenetic stimulation primarily affects neurons locally, which may lead to complex interactions between direct local effects on firing synchrony and indirect effects on inputs from neighboring regions. This may account for the observation that after optogenetic stimulation both SWA and synchrony measures declined, but not in a correlated manner. Moreover, the decline in SWA was significantly larger ipsi- than contralaterally (Figure 3G,H).

Changes in intrinsic excitability might also contribute to the decline of SWA after optogenetic stimulation. For instance, the non-inactivating hyperpolarization-activated cation current I_h plays a crucial role in the generation of the slow oscillation (McCormick and Bal, 1997, Blethyn et al., 2006). In the hippocampus, I_h is decreased by stimulation paradigms that induce LTD and increased by LTP (Fan et al., 2005, Brager and Johnston, 2007), but only in association with strong firing (theta bursts but not tetanus, which elicits few action potentials). However, while long-lasting homeostatic changes in intrinsic excitability mediated by I_h (Fan et al., 2005) might affect SWA after optogenetic stimulation, they cannot easily account for the associated decline of neuronal synchrony.

Several recent studies have shown that increased activation of specific cortical areas during wake results in a local increase in SWA during subsequent sleep, but in most cases it is not straightforward to tease apart the role of neuronal activity from that of synaptic plasticity (reviewed in (Hanlon et al., 2011)). However, a few studies contrasted conditions providing similar amounts of wake stimulation (activity) with or without a learning component (plasticity). In humans, SWA increased over right parietal cortex after a visuomotor task requiring learning compared to a kinematically identical task that did not require learning (Huber et al., 2004, Landsness et al., 2009). Similar results have been obtained using a reaching task in rodents and comparing the training and the post-training phase (Hanlon et al., 2009), indicating that changes in SWA reflect the effects of

synaptic plasticity above and beyond any effect of neuronal activity. Finally, a study in humans used transcranial paired-associative stimulation (PAS) in wake to deliver the same number of paired stimuli, but at time intervals meant to induce spike-timing dependent synaptic potentiation or depression, respectively (Huber et al., 2008). The potentiation paradigm locally increased SWA during subsequent sleep, whereas the depression paradigm decreased it, suggesting that changes in SWA are driven primarily by changes in synaptic plasticity, in line with the present results.

Conclusions

In summary, our findings demonstrate that sustained neuronal activation induced by active exploration in wake leads to an increase in SWA, neuronal synchrony, and neuronal OFF periods during subsequent sleep, consistent with the expected consequences of a net increase in synaptic strength in cortical circuits (Tononi and Cirelli, 2014). By contrast, a comparable, wake-like local increase in neuronal activity obtained by optogenetic stimulation during sleep was followed by a local decrease in SWA and neuronal synchrony, with no change in OFF periods. Thus, the increase in SWA and OFF periods after extended wake is unlikely to result from neuronal ‘fatigue’ induced by excessive firing as such. Instead, it appears that neuronal activation leads to homeostatic changes in sleep SWA only if it occurs in the neuromodulatory, metabolic, and neurochemical milieu of active wake, which influences multiple cellular functions including the ionic balance of interstitial spaces (Ding et al., 2016), and favors learning through synaptic potentiation (Tononi and Cirelli, 2014, de Vivo et al., 2016). Indeed, in previous studies we found that rats whose cortical noradrenergic levels had been depleted using chronic lesions of the locus coeruleus did not show the expected cortical induction of plasticity-related genes during wake, and had a blunted SWA response during subsequent sleep (Cirelli et al., 1996, Cirelli and Tononi, 2000, 2004, Cirelli et al., 2005). In the current study, the tone of the noradrenergic and other neuromodulatory systems was low because the mice were asleep, and thus laser-induced high firing occurred in a state that as a whole is not conducive to synaptic potentiation (Leonard et al., 1987, Bramham and Srebro, 1989). We cannot rule out, however, that laser stimulation also caused neurons to fire in a “random” pattern, uncoupled from wake behavior and physiological sensory inputs. While this may have contributed to the observed decrease in SWA after optogenetic stimulation, SSFO was chosen specifically to increase neuronal excitability while preserving as much as possible the endogenous pattern of firing. Finally, a recent study found that even ‘sleep-like’ slow waves occurring during

wake due to systemic atropine injections can lead to an increase in NREM sleep duration as long as subcortical areas are activated and the experimental animals are actively behaving (Qiu et al., 2015). This possibility should be tested further by experiments aimed at decoupling the effects of neuronal activity and plasticity during wake.

References

- Bellesi M, de Vivo L, Tononi G, Cirelli C (2015) Effects of sleep and wake on astrocytes: clues from molecular and ultrastructural studies. *BMC biology* 13:66.
- Benington JH, Heller HC (1995) Restoration of brain energy metabolism as the function of sleep. *Progress in Neurobiology* 45:347-360.
- Blethyn KL, Hughes SW, Toth TI, Cope DW, Crunelli V (2006) Neuronal basis of the slow (<1 Hz) oscillation in neurons of the nucleus reticularis thalami in vitro. *The Journal of neuroscience : the official journal of the Society for Neuroscience* 26:2474-2486.
- Borbély AA (1982) A two process model of sleep regulation. *Human Neurobiol* 1:195-204.
- Borbely AA, Baumann F, Brandeis D, Strauch I, Lehmann D (1981) Sleep deprivation: effect on sleep stages and EEG power density in man. *Electroencephalogr Clin Neurophysiol* 51:483-495.
- Borbely AA, Daan S, Wirz-Justice A, Deboer T (2016) The two-process model of sleep regulation: a reappraisal. *J Sleep Res.*
- Brager DH, Johnston D (2007) Plasticity of intrinsic excitability during long-term depression is mediated through mGluR-dependent changes in I(h) in hippocampal CA1 pyramidal neurons. *The Journal of neuroscience : the official journal of the Society for Neuroscience* 27:13926-13937.
- Brambilla D, Chapman D, Greene R (2005) Adenosine mediation of presynaptic feedback inhibition of glutamate release. *Neuron* 46:275-283.
- Bramham CR, Srebro B (1989) Synaptic plasticity in the hippocampus is modulated by behavioral state. *Brain research* 493:74-86.
- Brundage JM, Dunwiddie TV (1998) Metabolic regulation of endogenous adenosine release from single neurons. *Neuroreport* 9:3007-3011.
- Buzsaki G, Anastassiou CA, Koch C (2012) The origin of extracellular fields and currents--EEG, ECoG, LFP and spikes. *Nat Rev Neurosci* 13:407-420.
- Buzsaki G, Wang XJ (2012) Mechanisms of gamma oscillations. *Annu Rev Neurosci* 35:203-225.
- Chauvette S, Crochet S, Volgushev M, Timofeev I (2011) Properties of slow oscillation during slow-wave sleep and anesthesia in cats. *The Journal of neuroscience : the official journal of the Society for Neuroscience* 31:14998-15008.
- Cirelli C, Gutierrez CM, Tononi G (2004) Extensive and divergent effects of sleep and wakefulness on brain gene expression. *Neuron* 41:35-43.
- Cirelli C, Huber R, Gopalakrishnan A, Southard TL, Tononi G (2005) Locus ceruleus control of slow-wave homeostasis. *The Journal of neuroscience : the official journal of the Society for Neuroscience* 25:4503-4511.
- Cirelli C, Pompeiano M, Tononi G (1996) Neuronal gene expression in the waking state: a role for the locus coeruleus. *Science* 274:1211-1215.
- Cirelli C, Tononi G (2000) Differential expression of plasticity-related genes in waking and sleep and their regulation by the noradrenergic system. *The Journal of neuroscience : the official journal of the Society for Neuroscience* 20:9187-9194.
- Cirelli C, Tononi G (2004) Locus ceruleus control of state-dependent gene expression. *The Journal of neuroscience : the official journal of the Society for Neuroscience* 24:5410-5419.
- Dalsgaard MK, Secher NH (2007) The brain at work: a cerebral metabolic manifestation of central fatigue? *J Neurosci Res* 85:3334-3339.

- de Vivo L, Bellesi M, Marshall W, Bushong EA, Ellisman MH, Tononi G, Cirelli C (2016) Ultrastructural Evidence for Synaptic Scaling Across the Wake/sleep Cycle. *Science in press*.
- Ding F, O'Donnell J, Xu Q, Kang N, Goldman N, Nedergaard M (2016) Changes in the composition of brain interstitial ions control the sleep-wake cycle. *Science* 352:550-555.
- Esser SK, Hill SL, Tononi G (2007) Sleep homeostasis and cortical synchronization: I. Modeling the effects of synaptic strength on sleep slow waves. *Sleep* 30:1617-1630.
- Fan Y, Fricker D, Brager DH, Chen X, Lu HC, Chitwood RA, Johnston D (2005) Activity-dependent decrease of excitability in rat hippocampal neurons through increases in I(h). *Nature neuroscience* 8:1542-1551.
- Feinberg I, March JD, Fein G, Floyd TC, Walker JM, Price L (1978) Period and amplitude analysis of 0.5-3 c/sec activity in NREM sleep of young adults. *Electroencephalography and Clinical Neurophysiology* 44:202-213.
- Franken P, Malafosse A, Tafti M (1999) Genetic determinants of sleep regulation in inbred mice. *Sleep* 22:155-169.
- Grill WM (2008) Signal Considerations for Chronically Implanted Electrodes for Brain Interfacing. In: *Indwelling Neural Implants: Strategies for Contending with the In Vivo Environment* (Reichert, W. M., ed) Boca Raton (FL).
- Hanlon EC, Faraguna U, Vyazovskiy VV, Tononi G, Cirelli C (2009) Effects of skilled training on sleep slow wave activity and cortical gene expression in the rat. *Sleep* 32:719-729.
- Hanlon EC, Vyazovskiy VV, Faraguna U, Tononi G, Cirelli C (2011) Synaptic potentiation and sleep need: clues from molecular and electrophysiological studies. *Curr Top Med Chem* 11:2472-2482.
- Harley C (1991) Noradrenergic and locus coeruleus modulation of the perforant path-evoked potential in rat dentate gyrus supports a role for the locus coeruleus in attentional and memorial processes. *Progress in brain research* 88:307-321.
- Huber R, Deboer T, Tobler I (2000) Effects of sleep deprivation on sleep and sleep EEG in three mouse strains: empirical data and simulations. *Brain research* 857:8-19.
- Huber R, Ghilardi MF, Massimini M, Tononi G (2004) Local sleep and learning. *Nature* 430:78-81.
- Huber R, Maatta S, Esser SK, Sarasso S, Ferrarelli F, Watson A, Ferreri F, Peterson MJ, Tononi G (2008) Measures of cortical plasticity after transcranial paired associative stimulation predict changes in electroencephalogram slow-wave activity during subsequent sleep. *The Journal of neuroscience : the official journal of the Society for Neuroscience* 28:7911-7918.
- Landsness EC, Crupi D, Hulse BK, Peterson MJ, Huber R, Ansari H, Coen M, Cirelli C, Benca RM, Ghilardi MF, Tononi G (2009) Sleep-dependent improvement in visuomotor learning: a causal role for slow waves. *Sleep* 32:1273-1284.
- Leonard BJ, McNaughton BL, Barnes CA (1987) Suppression of hippocampal synaptic plasticity during slow-wave sleep. *Brain research* 425:174-177.
- Lovatt D, Xu Q, Liu W, Takano T, Smith NA, Schnermann J, Tieu K, Nedergaard M (2012) Neuronal adenosine release, and not astrocytic ATP release, mediates feedback inhibition of excitatory activity. *Proceedings of the National Academy of Sciences of the United States of America* 109:6265-6270.
- McCormick DA, Bal T (1997) Sleep and arousal: Thalamocortical mechanisms. *Annual Review of Neuroscience* 20:185-215.
- Musall S, von Pfostl V, Rauch A, Logothetis NK, Whittingstall K (2014) Effects of neural synchrony on surface EEG. *Cerebral cortex* 24:1045-1053.

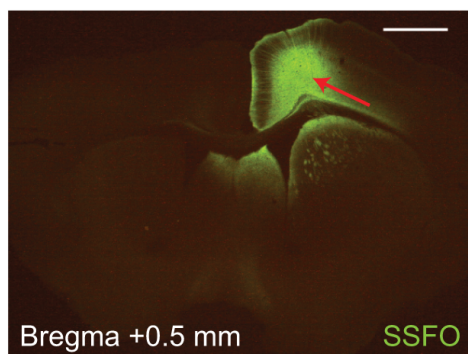
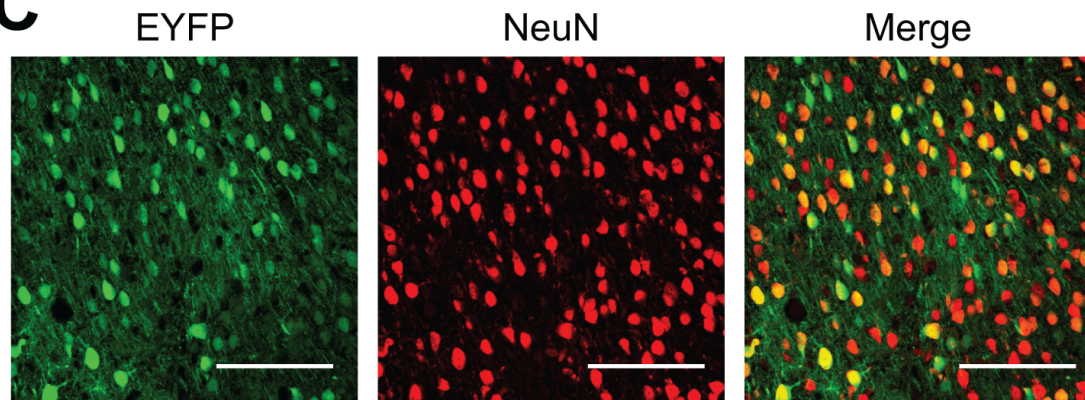
- O'Donovan MJ, Rinzel J (1997) Synaptic depression: a dynamic regulator of synaptic communication with varied functional roles. *Trends Neurosci* 20:431-433.
- Qiu MH, Chen MC, Lu J (2015) Cortical neuronal activity does not regulate sleep homeostasis. *Neuroscience* 297:211-218.
- Rechtschaffen A (1998) Current perspectives on the function of sleep. *Perspect Biol Med* 41:359-390.
- Seol GH, Ziburkus J, Huang S, Song L, Kim IT, Takamiya K, Huganir RL, Lee HK, Kirkwood A (2007) Neuromodulators control the polarity of spike-timing-dependent synaptic plasticity. *Neuron* 55:919-929.
- Steriade M, Timofeev I, Grenier F (2001) Natural waking and sleep states: a view from inside neocortical neurons. *Journal of neurophysiology* 85:1969-1985.
- Tononi G, Cirelli C (2006) Sleep function and synaptic homeostasis. *Sleep Med Rev* 10:49-62.
- Tononi G, Cirelli C (2012) Time to be SHY? Some comments on sleep and synaptic homeostasis. *Neural plasticity* 2012:415250.
- Tononi G, Cirelli C (2014) Sleep and the price of plasticity: from synaptic and cellular homeostasis to memory consolidation and integration. *Neuron* 81:12-34.
- Vyazovskiy VV, Harris KD (2013) Sleep and the single neuron: the role of global slow oscillations in individual cell rest. *Nat Rev Neurosci* 14:443-451.
- Vyazovskiy VV, Olcese U, Hanlon EC, Nir Y, Cirelli C, Tononi G (2011) Local sleep in awake rats. *Nature* 472:443-447.
- Vyazovskiy VV, Olcese U, Lazimy YM, Faraguna U, Esser SK, Williams JC, Cirelli C, Tononi G (2009) Cortical firing and sleep homeostasis. *Neuron* 63:865-878.
- Whittington MA, Cunningham MO, LeBeau FE, Racca C, Traub RD (2011) Multiple origins of the cortical gamma rhythm. *Dev Neurobiol* 71:92-106.
- Yizhar O, Fenno LE, Davidson TJ, Mogri M, Deisseroth K (2011) Optogenetics in neural systems. *Neuron* 71:9-34.

Figure 1. Experimental design. A. Representative example of virus expression in one mouse. Virus expression spread 2-3 mm in the anterior/posterior direction and remained within the right hemisphere. Red arrow denotes visible electrode tracks. Scale bar = 1mm. B. Placement of electrodes and screws in reference to the virus expression, as well as details of the microwire electrode array with 16 electrodes, of which only one row of 8 is shown. C. Example of EYFP (left) and NeuN (middle) expression in a confocal image taken near the injection site, and combined overlay of both images (right). Scale bars = 100 μ m. D. Experimental design. The two experiments (baseline+SD and baseline+laser-S) were spaced \sim 4-5 days apart and their order was counterbalanced. Vertical grey boxes indicate the time window in which most of the analysis was done, corresponding to the first 2 hours after SD or laser-S and the same time of day during baseline (hours 7-8 of the light period).

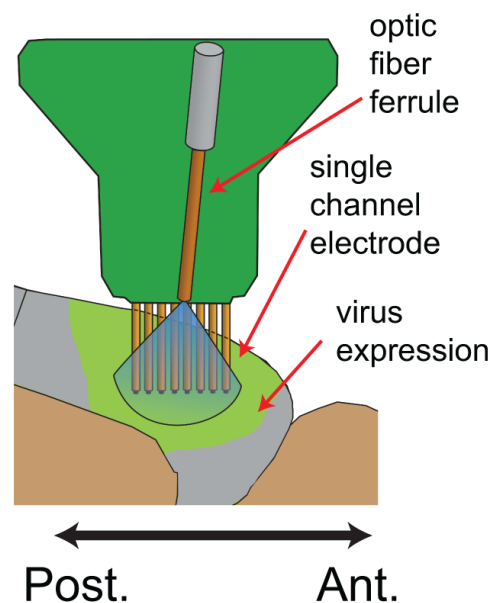
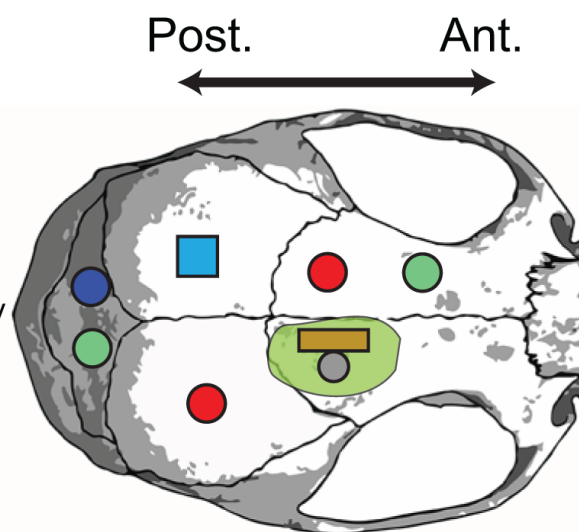
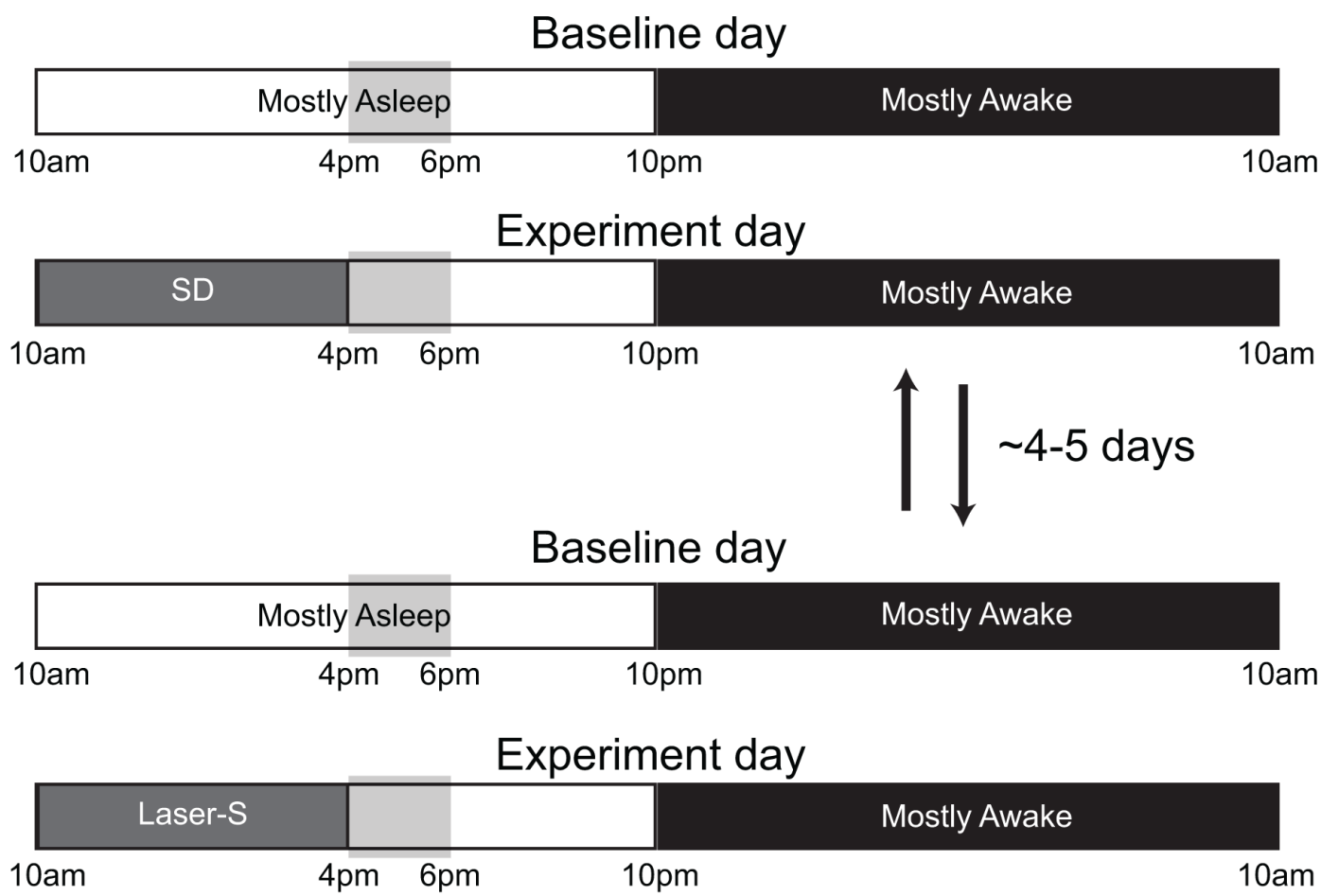
Figure 2. Sleep deprivation experiment. A. Left, firing rate in a representative electrode during the light period of baseline and SD days. Firing rate is plotted for each 4-sec epoch, and expressed as a percent of hours 1-12 NREM average firing rate during the baseline day. Right, firing rate for all electrodes during SD hours 1-6, plotted as percent change from the corresponding firing rate in baseline (59 electrodes, 16 mice). In this and the following boxplots, red and green lines denote median and mean, respectively; the blue box extends from the 25th to 75th percentile, and the black whiskers extend to 2.7 standard deviations. B. Left, mean spectrograms for frontal left EEG during hours 7-8 of the SD day (as % of total spectral power during hours 1-12 of the baseline day) (15 electrodes, 15 mice; Wilcoxon signed rank test, $p=6.10 \times 10^{-5}$). Here and in panel C, frequencies from 57-63 Hz are not displayed due to an artifact from a notch filter used to suppress 60 Hz electrical noise. Right, power in the SWA band (0.5-4 Hz) in NREM sleep during hours 7-8 of the SD day plotted as percent change from the corresponding baseline value. C. Same as in B, for ipsilateral (right) LFPs (59 electrodes, 16 mice; Wilcoxon signed rank test, $p=2.39 \times 10^{-11}$). D. Representative example of electrophysiological measures at \sim hour 7.5 in the baseline day and SD day. OFF periods are shown as gray bars under spike rasters. E. Average LFP waveform locked to all detected OFF periods from all electrodes in hours 7-8 of the SD day. F. OFF period measures after SD (hours 7-8) plotted as a percent change from the corresponding baseline. Number of OFF periods is per minute of NREM sleep (59 electrodes, 16 mice; Wilcoxon signed rank test, $p=0.0003$). Duration is the average duration of all OFF periods ($p=0.0001$). Percent of time spent in OFF periods is expressed as a percent of total time spent in NREM sleep ($p=4.44 \times 10^{-5}$). G. As F, for the first 2 hours of the dark period (hours 13-14) (59 electrodes, 16 mice; Wilcoxon signed rank test; Number: $p=0.03$, Duration: $p=0.52$, Percent: $p=0.05$). H. Correlation plot between firing rates during hours 1-6 of SD day and percent of NREM time spent in OFF periods in hours 7-8 of the same day for all 59 electrodes. 'r' shown is Pearson's rho, the black line is a least-squares fit (59 electrodes, 16 mice; Linear correlation; $r=0.64$ $p=4.72 \times 10^{-8}$).

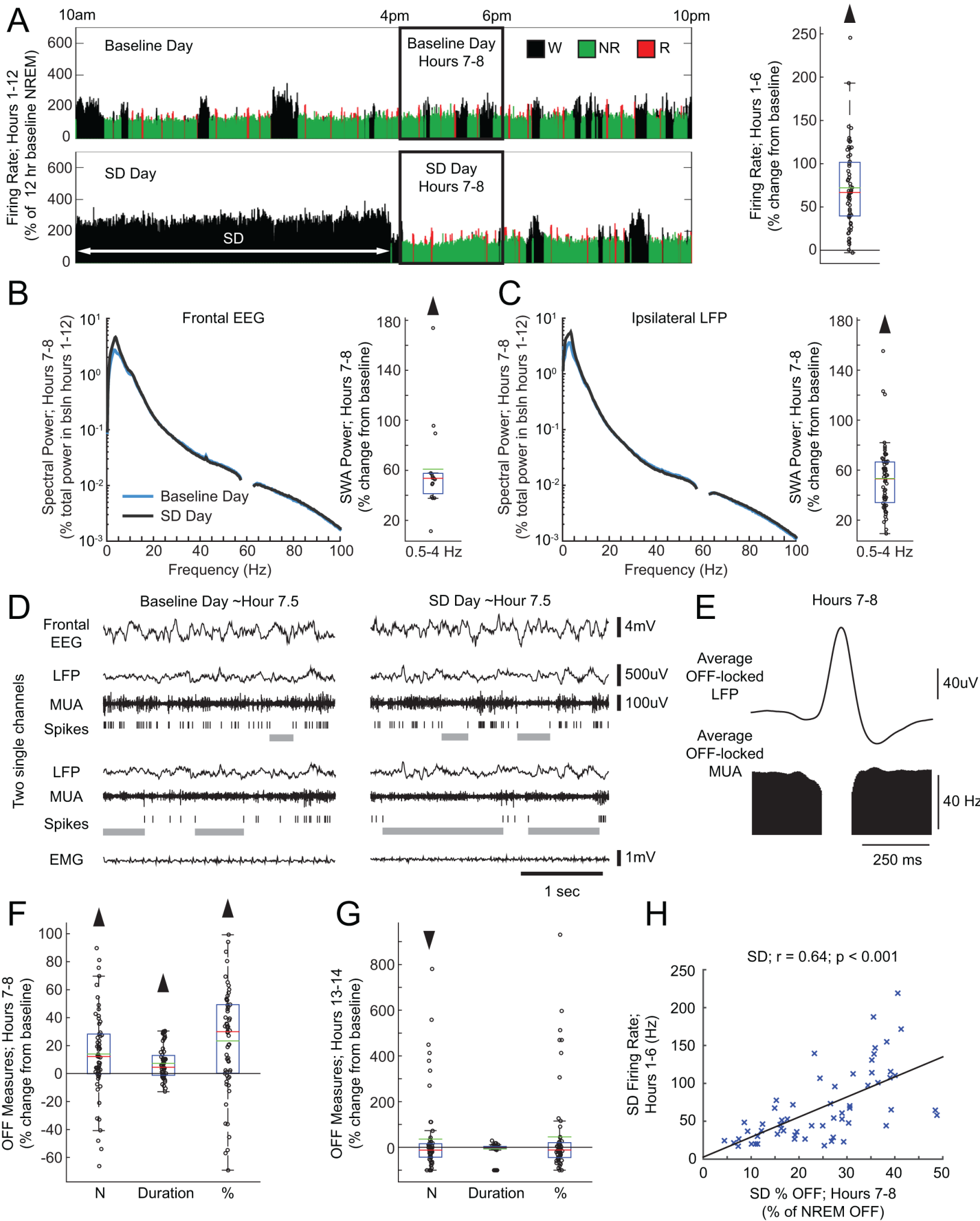
Figure 3. Laser-S experiment. A. Left, % of time spent in wake, NREM sleep and REM sleep in hours 1-6 (17 mice; Wilcoxon signed rank test; Wake: $p=0.55$, NREM: $p=0.24$, REM: $p=0.28$). Middle: average bout duration for wake and sleep in hours 1-6 (Wilcoxon signed rank test; Wake: $p=0.55$, NREM: $p=0.49$, REM: $p=0.08$), Right, number of brief awakenings (wake bouts ≤ 16 sec) per minute of NREM sleep in hours 1-6 (Wilcoxon signed rank test; $p=0.69$). All bars are mean, error bars show standard deviation. B. Left, mean spectrogram for frontal left EEG in hours 1-6 (% of total spectral power during hours 1-12 of the baseline day). Here and in other panels, frequencies from 57-63 Hz are not displayed due to an artifact from a notch filter used to suppress 60 Hz electrical noise. Right, power in SWA (0.5-4 Hz) and (30-55 Hz) bands for each frontal EEG in laser-S day plotted as percent change from the baseline day (15 electrodes, 15 mice; Wilcoxon signed rank test; SWA: $p=0.02$, Gamma: $p=0.03$). In this and the following boxplots, red and green lines denote the median and the mean, respectively; the blue box extends from the 25th to 75th percentile, and the black whiskers extend to 2.7 standard deviations. C. Representative example of electrophysiological measures in strong and weak responding electrodes at onset of laser stimulation. OFF periods are shown as gray bars under spike rasters. The blue box denotes the duration of a blue laser pulse. D. Left, firing rate in a representative strong responding electrode during the light period of the baseline and laser-S days. Firing rate is plotted for each 4-sec epoch, and expressed as a percent of hours 1-12 NREM average firing rate during the baseline day. Right, firing rate for all electrodes and SD-matched electrodes during laser-S hours 1-6, plotted as a percent change from the corresponding firing rate in baseline (Wilcoxon signed rank test; All: $n=66$, $p=8.82 \times 10^{-10}$, SD-matched: $n=32$, $p=7.95 \times 10^{-7}$). E. OFF period measures during hours 1-6 of laser-S for SD-matched electrodes. Percent change in laser-S from the baseline day is plotted for each OFF measure. Number of OFF periods is per minute of NREM sleep (32 electrodes, 11 mice; Wilcoxon signed rank test, $p=7.95 \times 10^{-7}$). Duration is the average duration of all OFF periods ($p=7.95 \times 10^{-7}$). Percent of time spent in OFF periods is expressed as a percent of total time spent in NREM sleep ($p=7.95 \times 10^{-7}$). F. Left, mean spectrogram for the LFPs of SD-matched electrodes during hours 1-6 (% of total spectral power during hours 1-12 of the baseline day) (32 electrodes, 11 mice; Wilcoxon signed rank test; Delta: $p=7.95 \times 10^{-7}$, Gamma: $p=7.95 \times 10^{-7}$). Right, power in SWA and gamma bands for the laser-S day plotted as percent change from the baseline. Note that the spectrograms shown are all scaled uniformly 0-100 Hz by a single value, the total power across all frequency bins in the baseline day hours 1-12. G. Left, mean spectrograms for frontal EEG during hours 7-8 of the laser-S day (% of total spectral power during hours 1-12 of the baseline day). Right, power in the SWA and gamma bands plotted as percent change from the baseline (9 electrodes, 9 mice; Wilcoxon signed rank test, Delta: $p=0.03$ Gamma: $p=0.91$). H. Same as in G for the LFPs of SD-matched electrodes (32 electrodes, 11 mice; Wilcoxon signed rank test; SWA: $p=6.59 \times 10^{-7}$, Gamma: $p=0.24$). I. Average LFP waveform in SD-matched electrodes locked to all detected OFF from all electrodes in hours 7-8 of the laser-S day. J. OFF period measures in SD-matched electrodes after laser-S (hours 7-8) plotted as a percent change from the corresponding baseline. Number of OFF periods is per minute of NREM sleep (32 electrodes, 11 mice; Wilcoxon signed rank test, $p=0.68$). Duration is the average duration of all OFF periods ($p=0.91$). Percent of time spent in OFF periods is expressed as a percent of total time spent in NREM sleep ($p=0.55$). K. Correlation plot between firing rates during hours 1-6 of laser-S day and percent of time spent in OFF periods in hours 7-8 for SD-matched electrodes. 'r' shown is Pearson's rho, the black line is a least-squares fit (59 electrodes, 16 mice; Linear correlation; $r=-0.04$ $p=0.81$). L. As in J, for all ipsilateral electrodes in Laser-S (66 electrodes, 17 mice; Wilcoxon signed rank test; Number: $p=0.34$, Duration: $p=0.19$, Percent: $p=0.28$).

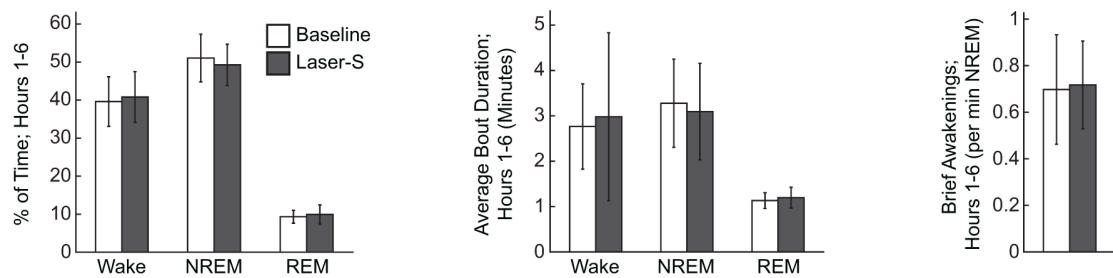
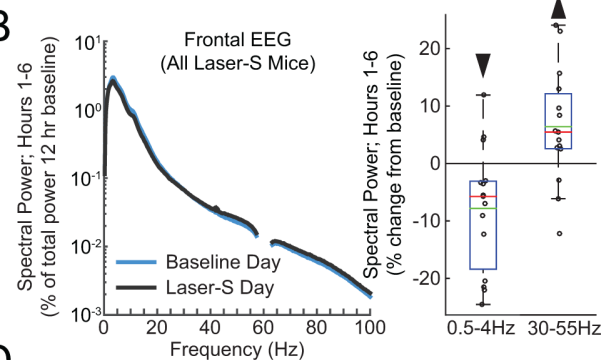
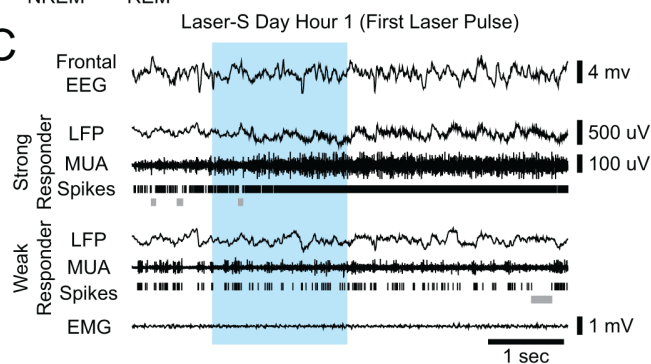
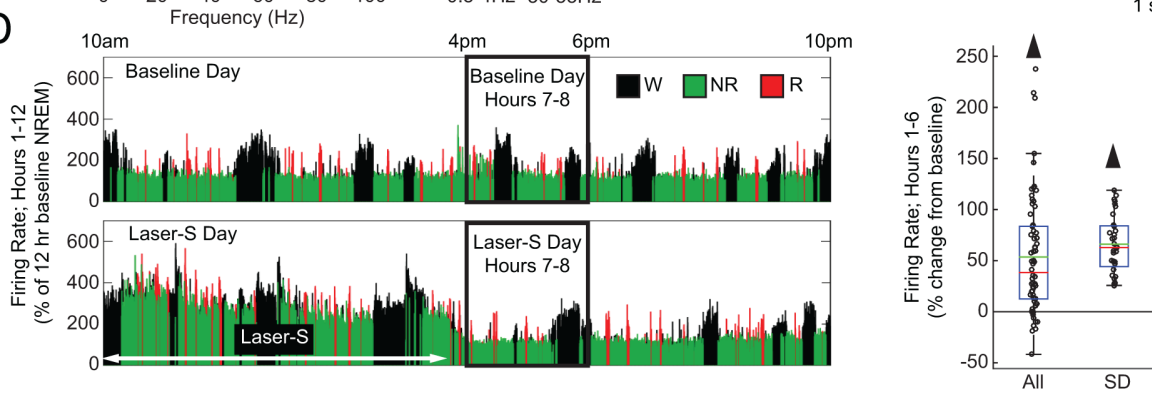
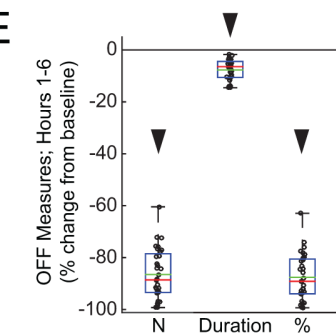
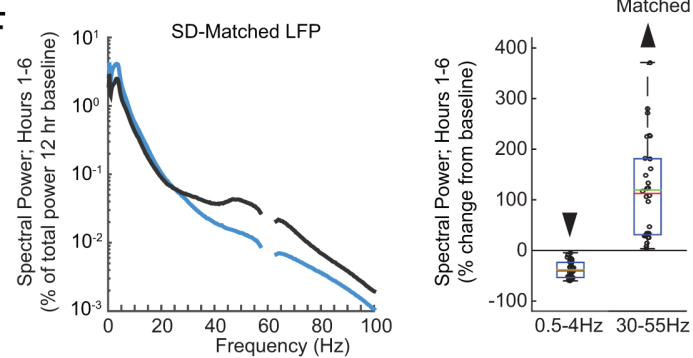
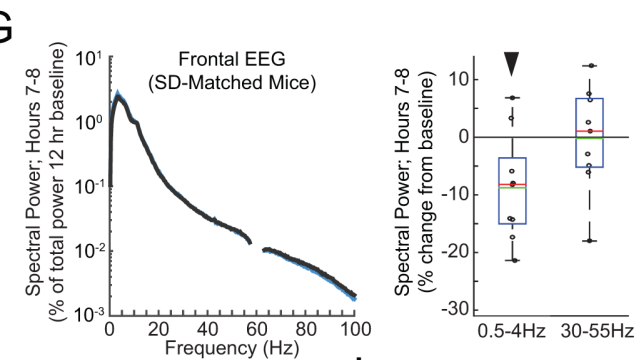
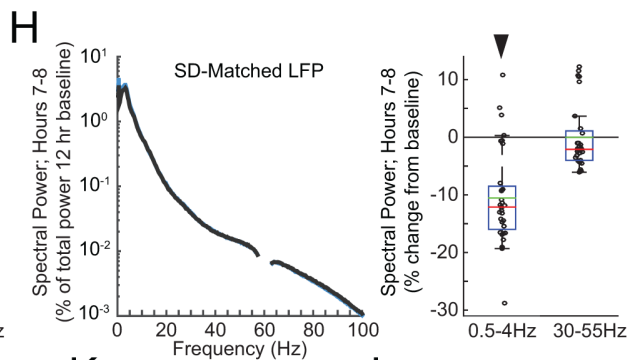
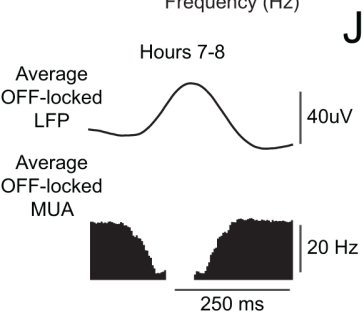
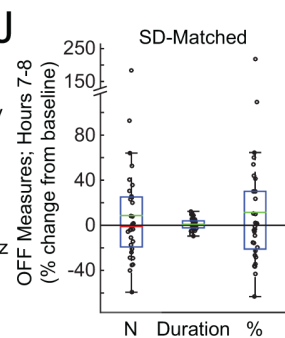
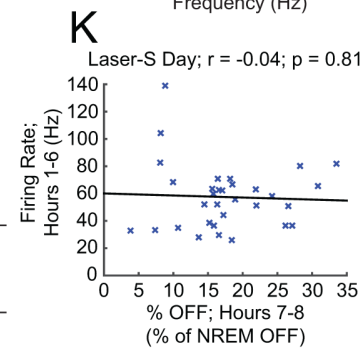
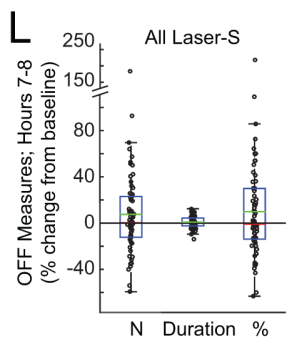
Figure 4. Changes in ON period synchrony after SD and laser stimulation. A. Examples of synchrony measurements across the onset and offset of ON periods. The top electrode is the one being evaluated (the target electrode), with ON periods (spikes) shown in red and OFF periods shown in blue. In the other 5 electrodes of the same array, spikes are shown in black, except when a corresponding ON period starts or ends in synchrony with the target electrode, in which case spikes are shown in red. Synchrony was measured within a window of 48 ms centered over the beginning and ending of the ON periods of the target electrode (yellow area). For better visualization, the size of this window is not drawn to scale. Note that only the start and end of ON periods count as possible synchrony events, and that shorter silences within an ON period that do not pass the OFF period threshold are not ON period boundaries. B. Synchrony measures in hours 7-8 after SD, shown for each electrode as a percent of the synchrony in the baseline day hours 7-8 (55 electrodes, 12 mice; Wilcoxon signed rank test; ON Starts: $p=1.72 \times 10^{-6}$, ON Ends: $p=6.51 \times 10^{-8}$). In the boxplots, data points are shown as black circles, red and green lines denote the median and the mean, respectively; the blue box extends from the 25th to 75th percentile, and the black whiskers extend to 2.7 standard deviations from the mean. C. Correlation plot between average LFP SWA and average synchrony for start of ON periods in hours 7-8 of the SD day for all 12 mice used for synchrony analysis. 'r' shown is Pearson's rho, the black line is a least-squares fit (12 mice; Linear correlation; $r=-0.84$ $p=0.0006$). E. Correlation plot between average LFP SWA and average synchrony for start of ON periods in hours 7-8 of the laser-S day (9 mice; Linear correlation; $r=-0.04$ $p=0.93$). D. As in B, for laser-S electrode subsets (SD-matched: 30 electrodes, 9 mice; Wilcoxon signed rank test; ON Starts: $p=0.03$, ON Ends: $p=0.37$) (All Laser-S: 63 electrodes, 14 mice; Wilcoxon signed rank test; ON Starts: $p=0.001$, ON Ends: $p=0.04$). F. As in B, for contralateral laser-S electrodes (22 electrodes, 5 mice; Wilcoxon signed rank test; ON Starts: $p=0.66$, ON Ends: $p=0.12$).

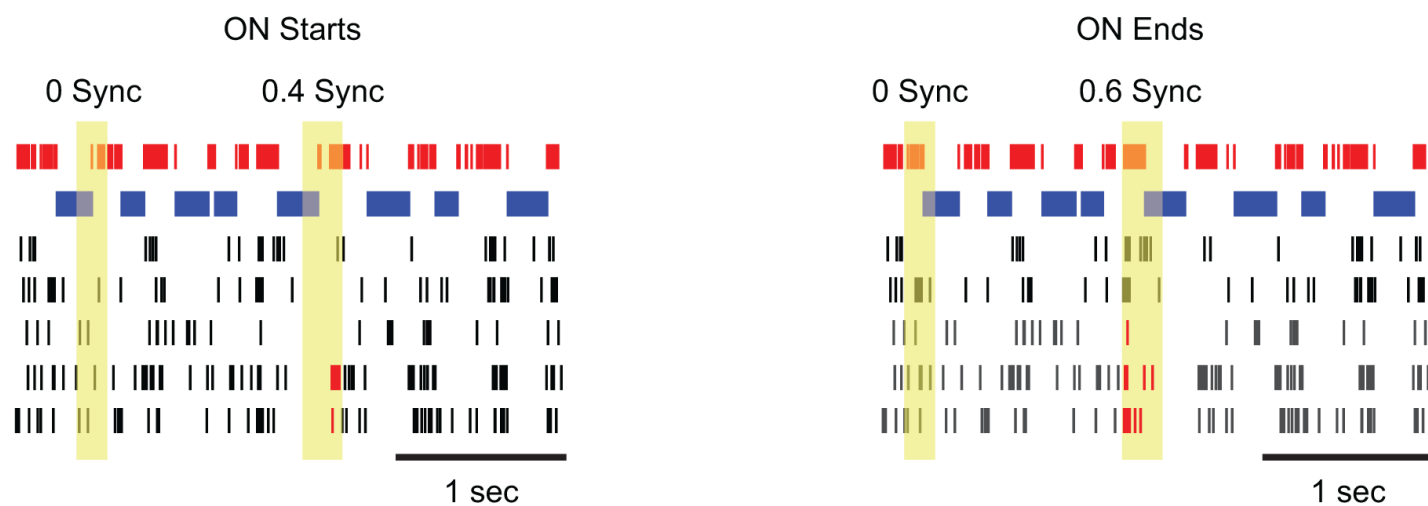
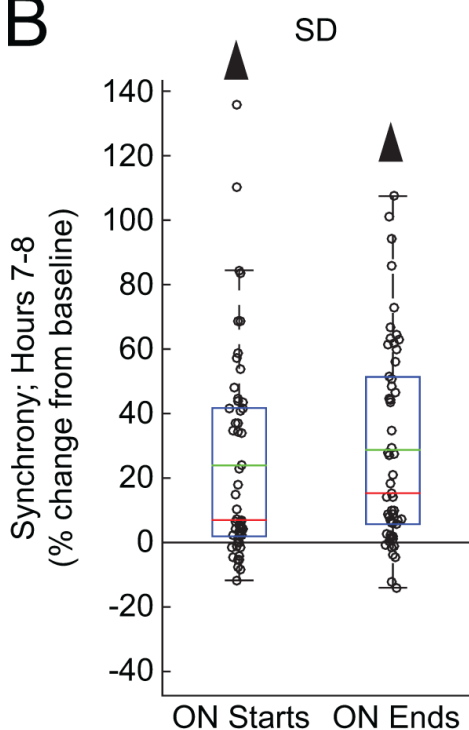
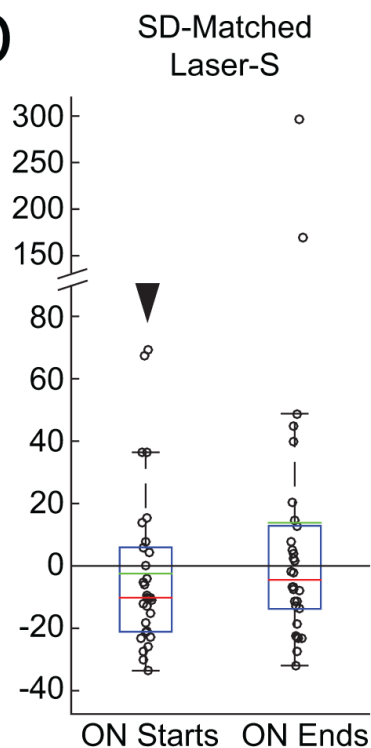
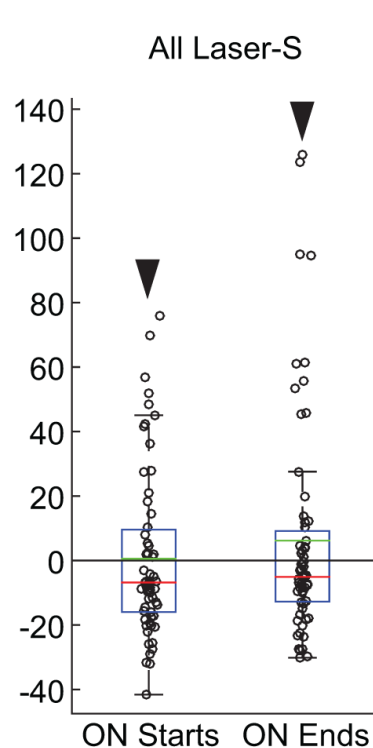
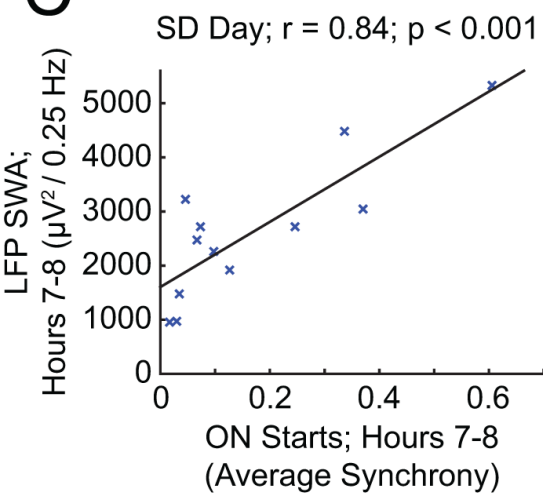
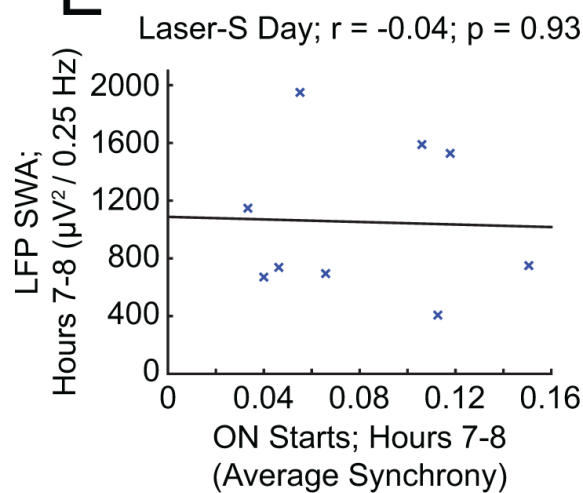
A**C****B**

- Virus expression
- Ipsilateral electrode array
- Optic fiber ferrule
- Contralateral electrode array
- EEG screw
- Reference screw
- Anchor screw

**D**



A**B****C****D****E****F****G****H****I****J****K****L**

A**B****D****E****C****E****F**